J Solid State Electrochem (2010) 14:1885–1895
DOI 10.1007/s10008-010-1015-y

ORIGINAL PAPER

Oxygen addition effects on electrochromic properties of PECVD-synthesized WO_xC_y films for flexible electrochromic devices

Yung-Sen Lin · Hsuan-Ta Chen · Siang-Syuan Wu

Received: 16 November 2009 / Revised: 21 January 2010 / Accepted: 27 January 2010 / Published online: 2 March 2010

Abstract An investigation was conducted into the electrochromic properties of organotungsten oxide WO_xC_y films synthesized onto 60 Ω/□ flexible polyethylene terephthalate/indium tin oxide substrates using low temperature, plasma-enhanced chemical vapor deposition (PECVD) at varying oxygen concentrations. The PECVD-synthesized WO_xC_y films were proven to offer remarkable electrochromic performance. Cyclic voltammetry switching measurements revealed that only low driving voltages from −1 to 1 V are needed to provide reversible Li^+ ion intercalation and de-intercalation in a 0.1 M $LiClO_4$–PC electrolyte. Light modulation with transmittance variation of up to 72.9% and coloration efficiency of 62.5 cm^2/C at a wavelength of 650 nm was obtained.

Keywords PECVD · Flexible substrate · Electrochromic materials · Tungsten oxide · Cyclic voltammetry

Introduction

Transition metal oxides have attracted growing interest for their numerous applications in electrochromic (EC) and related devices such as photovoltaic-powered EC smart windows, photo-EC devices, gas sensors, EC displays [1], EC sunroofs [2], and EC mirrors [3]. Three major configurations of EC devices such as battery-like, solution phase-like, and hybrid structure-like are reported [4]. EC devices with configurations of solution phase and hybrid structure are so-called self-erasing types, in which one or both of the color-changing electrochromic substances is dissolved in a liquid or gel electrolyte, where they can freely diffuse. EC devices with battery-like configuration have extended open circuit memory. A continuous current is required to maintain the self-erasing devices in the colored state, with the depth of coloration being proportional to the current density. In battery-like EC devices, electrochromic thin film and counter electrode coat the optically transparent electrodes and an ion conducting, electronically insulating electrolyte separates them. Electrolyte is either a polymer/gel or a thin film. Polymer/gel electrolyte leads to laminated sandwich structures while thin film electrolytes are the basis of all-thin-film electrochromic coatings [4]. Battery-like EC devices with built-in laminated or monolithic demonstration devices on glass are produced. One of the current aims in the EC device industry is to industrialize EC device fabrication to obtain rapidly produced large-area windows with low production costs and excellent durability. Battery-like EC devices have been investigated for flexible substrate application [5]. Such flexible EC devices present the specific advantage of versatile shapability.

Tungsten oxide (WO_x) has remained the most promising candidate for large-scale uses of electrochromic devices [1]. WO_x film in a bleached state (colorless) can be reversed to a colored state (dark blue) by intercalation of ions and electrons to form tungsten bronze ($M_\alpha WO_x$) according to the intercalation/de-intercalation reaction (1) [6]:

$$WO_x + \alpha M^+ + \alpha e^- \leftrightarrow M_\alpha WO_x \quad (1)$$

where M^+ denotes H^+, Li^+, Na^+, or K^+ ions.

Electrochromic tungsten oxide films have been prepared by a variety of methods, including sol–gel deposition [7], electrodeposition [8], spray pyrolysis [9], evaporation [10], sputtering [11], laser ablation deposition [12], chemical

Y.-S. Lin (✉) · H.-T. Chen · S.-S. Wu
Department of Chemical Engineering, Feng Chia University,
No.100, Wenhwa Road, Seatwen,
Taichung, Taiwan 407, Republic of China
e-mail: yslin@fcu.edu.tw

vapor deposition (CVD) [13], and plasma-enhanced CVD (PECVD) [14]. Electrochromism of WO_x film has been intensively studied over the last 30 years, but questions still remain regarding scale-up [15] and irreversible Li^+ trapping by water and hydroxyl ions [16]. If electrochromic WO_x film can be deposited onto flexible polyethylene terephthalate (PET)/indium tin oxide (ITO) substrate by roll-to-roll PECVD deposition, then the issues regarding scale-up and irreversible Li^+ trapping by water and hydroxyl ions can be solved. Most of the previous studies have employed tungsten oxide films deposited onto rigid substrates. Deposition of electrochromic WO_xC_y films onto flexible PET/ITO substrates by PECVD has not yet been studied and is the subject of this investigation. This study attempts to use low temperature (23 °C) PECVD process with a precursor [tungsten carbonyl, $W(CO)_6$; TC] and air gas to deposit electrochromic WO_xC_y films onto flexible PET/ITO substrates. Effects of oxygen concentrations on electrochromic properties of PECVD-synthesized WO_xC_y films were investigated. The electrochromic performance of flexible PET/ITO/PECVD-synthesized WO_xC_y was evaluated by electrochemical and transmittance measurements. To understand how the electrochromism of WO_xC_y films is affected by the properties of WO_xC_y films, the properties of WO_xC_y films were studied by field emission scanning electron microscopy (FESEM), Raman spectroscopy, and X-ray photoelectron spectroscopy (XPS).

Experimental details

PECVD-synthesized WO_xC_y films

WO_xC_y films were synthesized onto flexible PET/ITO substrates (60 Ω/□, 125 μm thick, 3 cm×6 cm) by a low temperature PECVD, which was accomplished in a custom-built PECVD chamber. When the pressure of the plasma chamber was pumped down to less than 5 mTorr and the pressure leakage rate was less than 0.1 mTorr/min (i.e., the leakage flow rate of air into the chamber was less than 1% of the flow rate of the inlet gases), Ar gas (99.9% pure)-carried TC vapor (with gas line heated to 110 °C), and air gas (99.9% pure) were fed into the plasma chamber. TC vapor was obtained by heating precursor TC solid (99% pure) in a tank at 110 °C. TC solid was stored and transferred to a cool, dry, well-ventilated area away from heat and direct sunlight. Ar at 4 sccm, TC at 4 sccm, and various oxygen concentrations (at air flow rates of 1.2, 2.2, 4.5, and 8.9 sccm) were set, respectively, as shown in Table 1. When the chamber pressure stabilized at 12 Pa (90 mTorr), r.f. (13.56 MHz) and 200 W of power were applied to create the plasmas. PET/ITO substrates were exposed directly to the plasmas for 8 min. After deposition, the r.f. power was turned off. Gases were pumped out and system pressure returned to background pressure (around 5 mTorr). The vacuum was broken by opening a valve to admit air into the chamber. Once the chamber pressure reached atmospheric pressure (typically within 5 min), flexible PET/ITO/WO_xC_y was taken out for measurements.

Table 1 Settings for deposition of WO_xC_y films onto PET/ITO substrates by PECVD

Parameters	Settings			
Power (W)	200			
Ar flow rate (sccm)	4			
TC flow rate (sccm)	4			
Chamber pressure (Pa)	12			
Exposed duration (min)	8			
Oxygen concentration (%)	2.7	4.5	7.6	11.1
Air flow rate (sccm)	1.2	2.2	4.5	8.9

Thin film analysis

Two-dimensional (2D) surface morphology and thickness of WO_xC_y films were observed from the top surfaces and cross sections using FESEM. The porosity of the surface of each sample can be interpreted by the grain boundary fraction (%) of FESEM image on the top surface. A high grain boundary fraction (%) refers to high porosity. The grain boundary fraction (%) of the surface of each sample was calculated by dividing the area of grain boundary by the total area of coatings on the FESEM images using the Image-Pro Plus Version 4.5.0.29 software (purchased from Media Cybermetics, Inc). The variation in grain boundary fraction (%) of the analyzed samples was found to be less than 5% for five repeated analyses of FESEM image on the selected surface.

Deposition rates of PECVD-synthesized WO_xC_y film were determined by film thickness (from FESEM image on the cross section) divided by the duration of deposition. FESEM images were collected on a HITACHI S-4800. The system was equipped with an electron gun emitting a cold field with an electrical voltage of 1 kV and an electrical current of 5 μA. Data were recorded for a scan area of 500 nm with 1,024×840 pixels. The variation in thickness and deposition rate between samples was less than 5%.

Raman spectra of the specimen were obtained using a diode type of Ar^+ laser of 785 nm wavelength (Renishaw, Model inVia Raman microscope).

Thermo VG Scientific Sigma Probe and the XPS system were equipped with an Al Kα X-ray source at 1,486.6 eV, with pass energy at 50 eV and charge compensation at 0.4 mA, to compositionally analyze samples. Both survey and high-resolution modes of XPS data were collected. Data were recorded at a 53° collecting angle while high-resolution spectra

had a spot size of 400 μm and analytic depths of ~5 nm. The following binding energies for WO_xC_y coatings were analyzed: $W^{6+}_{4f7/2}$ and $W^{6+}_{4f5/2}$ at 35.1 and 37.2 eV; $W^{5+}_{4f7/2}$ and $W^{5+}_{4f5/2}$ at 33.9 and 36.4 eV; C_{1s} (C–C at 284.4 eV and C–O at 286.1 eV); O_{1s} (WO_3 at 529.9 eV, $WO_{2.5}$ at 529.85 eV, and C–O at 532 eV). The variation in the proportions of W^{5+} and W^{6+} in the samples was less than 10%.

Electrochemical characterization

Cyclic voltammetric measurements were performed by a Jiehan 5000 electrochemical station. Flexible PET/ITO/WO_xC_y was mounted on a working electrode. A Pt grid was used as a counter electrode. The electrolyte was a 0.1 M $LiClO_4$–PC solution. Cyclic voltammograms (CVs) were recorded at a scan rate of 50 mV/s, between −1 and 1 V versus the reference electrode, which was a saturated calomel electrode $Hg/Hg_2Cl_2/KCl$ (saturated in water). A glass cell filled with the electrolyte and containing the Pt grid was taken as the background. Transmittance of PET/ITO/WO_xC_y was measured by a Labguide DH2000-BAL spectrophotometer.

Electrochromic performance of flexible PET/ITO/PECVD-synthesized WO_xC_y was determined in terms of transmittance variation (ΔT), optical density change (ΔOD), and color efficiency (η) by Eqs. 2, 3, and 4:

$$\Delta T(\%) = T_{\text{bleached}}(\%) - T_{\text{colored}}(\%) \tag{2}$$

$$\Delta OD = \log\left[\frac{T_{\text{bleached}}(\%)}{T_{\text{colored}}(\%)}\right] \tag{3}$$

$$\eta = \frac{\Delta OD}{q} \tag{4}$$

where T_{bleached} (%) and T_{colored} (%) denote the transmittance of the samples in the bleached state (ion de-intercalation state) and colored state (ion intercalation state), respectively, and q denotes the charge intercalation per unit area. In this study, experiments were repeated five times. The variations in transmittance variation (ΔT), optical density change (ΔOD), and color efficiency (η) between the prepared samples were controlled at less than 10%.

Intercalation coefficient α_i and de-intercalation coefficient α_d

The quantities α_i and α_d are termed the intercalation coefficient and de-intercalation coefficient of Li^+ ions, respectively, and are calculated by Eqs. 5, 6, and 7:

$$\alpha_i\,;\,\alpha_d = \frac{M_{Li^+}}{M_{WO_xC_y}} \tag{5}$$

$$M_{Li^+} = \frac{(q/q_{e^-})}{N} \tag{6}$$

$$M_{WO_xC_y} = \frac{V \times D}{m} \tag{7}$$

where M_{Li^+} denotes the moles of Li^+ intercalated (de-intercalated), $M_{WO_xC_y}$ denotes the moles of WO_xC_y film, V denotes the film volume, D denotes the film density, m denotes the molecular weight of WO_xC_y, q denotes the charge of Li^+ intercalated (de-intercalated), q_{e^-} denotes the charge of electron intercalated (de-intercalated), and N is Avogadro's number. The variation in intercalation coefficient α_i and de-intercalation coefficient α_d between the prepared samples was less than 10%.

Results and discussion

Surface morphology and film properties

Electrochromic performance of electrochromic films was proven to be highly affected by their surface properties in our previous study [17]. This is because Li^+ intercalation (see Fig. 1a) and de-intercalation (see Fig.1b) in a 0.1 M $LiClO_4$–PC electrolyte occur on the surfaces before Li^+ goes deeper into the film. FESEM images of PET/ITO/PECVD-synthesized WO_xC_y films at oxygen concentrations of 2.7–11.1% are shown in Figs. 2a–d. The porosity on the top surfaces of PECVD-synthesized WO_xC_y films in Figs. 2a–d can be illustrated as the ranking of the grain boundary fraction ε (%) dependent on oxygen concentrations: $\varepsilon_{7.6\%}$ (33.1±1.7%)>$\varepsilon_{11.1\%}$ (24.1±1.2%)>$\varepsilon_{4.5\%}$ (18.1±0.9%)>$\varepsilon_{2.7\%}$ (12.5±0.6%). This indicates that PECVD-synthesized WO_xC_y films at an oxygen concentration of 7.6% provide the most porous surface, as the highest determined grain boundary fraction is 33.1±1.7% (see Fig. 2c). Lower grain boundary fraction ε (%) was observed at oxygen concentrations of higher or lower than 7.6%.

Figure 3 shows the lowest values for deposition rate (45.1±2.3 nm/min) and thickness (361±18 nm) of WO_xC_y film obtained at an oxygen concentration of 7.6%, resulting in the most porous surface, as shown in Fig. 2c. In contrast, higher deposition rates and thicknesses at oxygen concentrations of 2.7%, 4.5%, and 11.1% are shown in Fig. 3, with less porous surfaces, as shown in Fig. 2a, b, and d.

Figure 4 shows two relatively sharp peaks centered at 723 and 950 cm^{-1}, and three broad peaks centered at 365, 500, and 793 cm^{-1}, respectively, on Raman spectra of PECVD-synthesized WO_xC_y films at various oxygen concentrations. The sharp peak at 950 cm^{-1} was assigned to the W^{6+}═O stretch mode of terminal oxygen. This is the so-

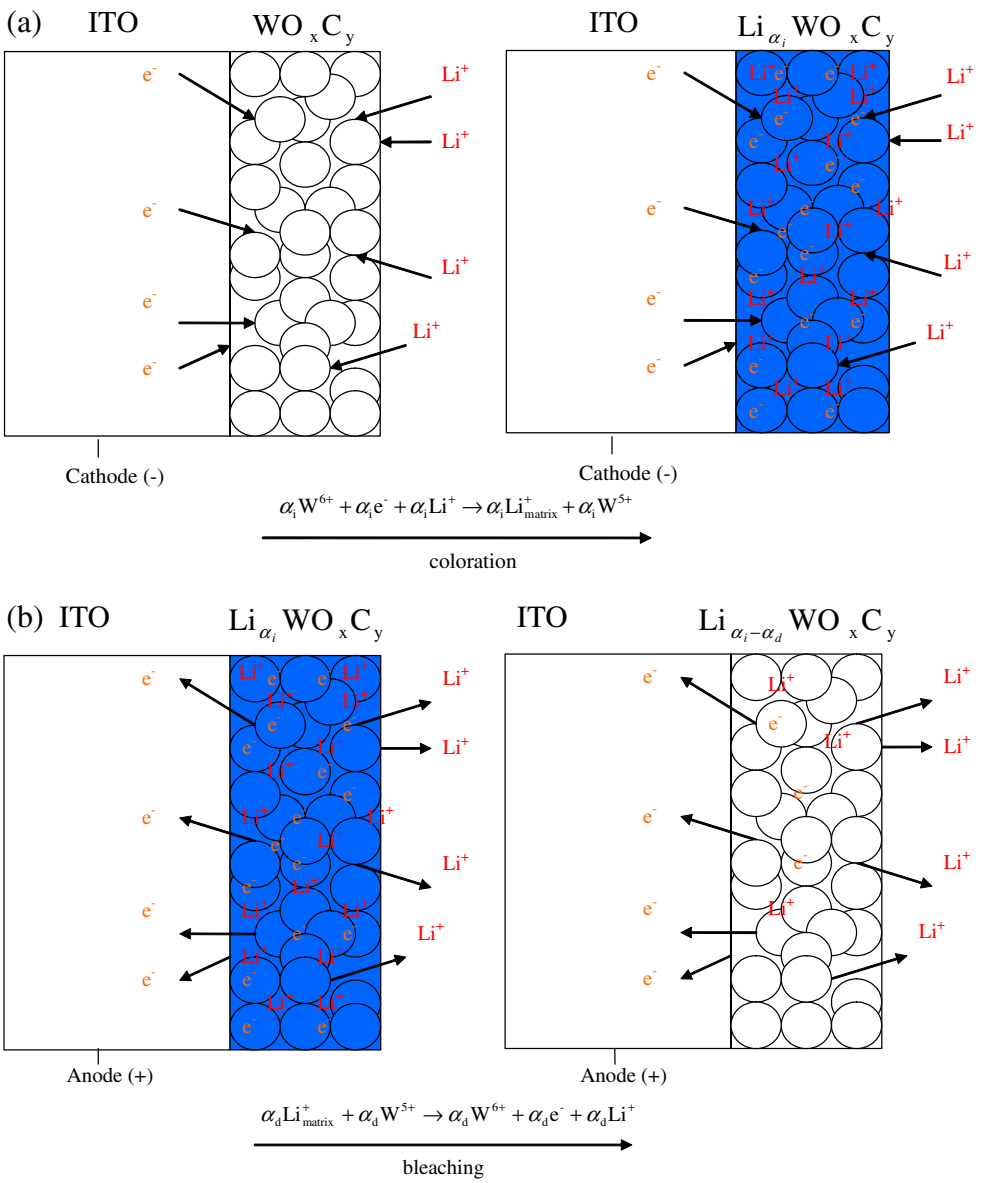

Fig. 1 Schematic of ITO/WO_xC_y shown during **a** Li^+ intercalation (coloration) and **b** Li^+ de-intercalation (bleaching) of the inorganic matrix

called double tungsten oxygen bond W^{6+}=O, possibly on the surface of the cluster or in the micro-void structures in the film [18]. Double bond W=O is stronger than W–O single bond. The vibration frequency of W=O double bond is expected to be higher than that of W–O single bond. The peaks between 200 and 400 cm^{-1} are O–W–O bending modes, while W–O stretching modes originate in the peaks between 600 and 1,000 cm^{-1} [19]. Hence, the peaks at 793 and 723 cm^{-1} correspond to the W^{6+}–O stretching modes of edge sharing oxygen such as O–W^{6+}–O single bond [20] and W^{6+}–O–W^{6+} single bond [21], respectively. In Fig. 4, broad peaks near 365 and 500 cm^{-1} are presented, which are respectively related to the bending modes of O–W^{5+}–O single bond and W^{5+}=O double bond in WO_xC_y films, since these bonds are weaker than the bonds involving W^{6+} ions. Their corresponding Raman peaks appear at lower energies than those for the W^{6+}–O and W^{6+}=O bonds [22]. Figure 4 shows that the lower the oxygen concentration, the higher the numbers of O–W^{5+}–O single bonds and W^{5+}=O double bonds produced in WO_xC_y films. The W^{6+}=O and W^{5+}=O stretching modes in WO_xC_y films suggest that PECVD-synthesized WO_xC_y films at oxygen concentration of 2.7–11.1% are amorphous as a crystal does not have any double bonds [23].

Li^+ ion intercalation and de-intercalation

Figure 5 shows the CVs of WO_xC_y films synthesized on flexible PET/ITO substrates at various oxygen concentrations for Li^+ intercalation and de-intercalation in a 0.1 M $LiClO_4$–PC electrolyte at a scan rate of 50 mV/s from −1.0 to 1.0 V. The current density of CVs indicates the amount

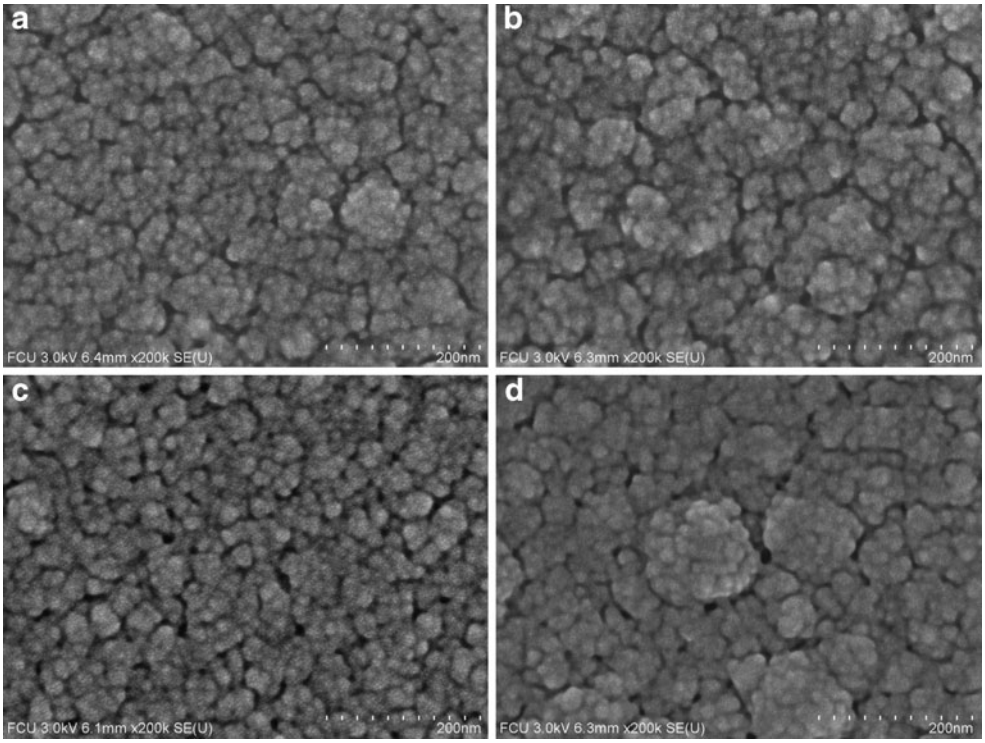

Fig. 2 FESEM images of PET/ITO/WO_xC_y films synthesized by PECVD at oxygen concentrations of **a** 2.7%, **b** 4.5%, **c** 7.6%, and **d** 11.1%

of electrons flowing into and out of WO_xC_y films in conjunction with Li^+ ion intercalation/de-intercalation per unit time period (s) and unit area (cm^2) at certain potential. The cathodic peak current density i_{pc}, cathodic peak potential E_{pc}, anodic peak current density i_{pa}, and anodic peak potential E_{pa} in Fig. 5 are listed in Table 2. Table 2 shows that the largest values for i_{pc} (0.64 mA/cm^2, at cathodic peak potential at −0.998 V) and i_{pa} (0.40 mA/cm^2, at anodic peak potential at −0.044 V) were obtained at an optimal oxygen concentration of 7.6%. An optimal oxygen concentration of 7.6% gives the most porous surface (see Fig. 2c) of synthesized WO_xC_y film at grain boundary fraction of 33.1%. The porous surfaces of WO_xC_y films allow Li^+ to be intercalated easily from 0.1 M $LiClO_4$–PC electrolyte to the surfaces of WO_xC_y films and allow Li^+ to be de-intercalated easily from the surface of $Li_{x_i}WO_xC_y$ films to 0.1 M $LiClO_4$–PC electrolyte. This results in the highest i_{pc} and i_{pa}. When the oxygen concentration is increased to 11.1%, the surface shows a slight decrease in porosity with a grain boundary fraction of 24.1%, resulting in a slight decrease in the values of i_{pc} (0.6 mA/cm^2) and i_{pa} (0.38 mA/cm^2). If the oxygen concentrations significantly decrease to 2.7–4.5%, the surface porosity significantly decreases to grain boundary fraction of 12.5–18.0%, resulting in a significant decrease in the values of i_{pc} (0.44–0.45 mA/cm^2) and i_{pa} (0.25–0.28 mA/cm^2).

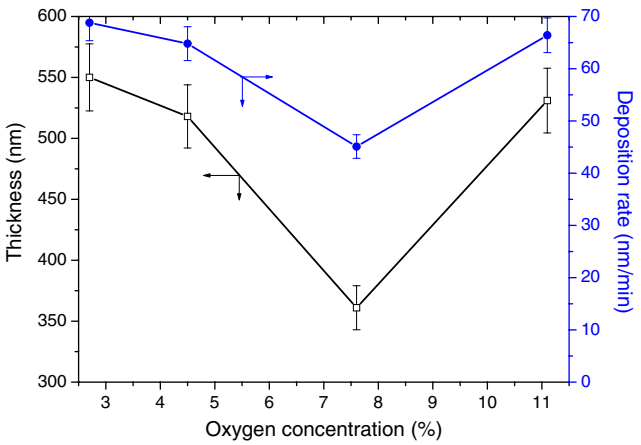

Fig. 3 The thickness and deposition rates of PET/ITO/WO_xC_y films as a function of oxygen concentration

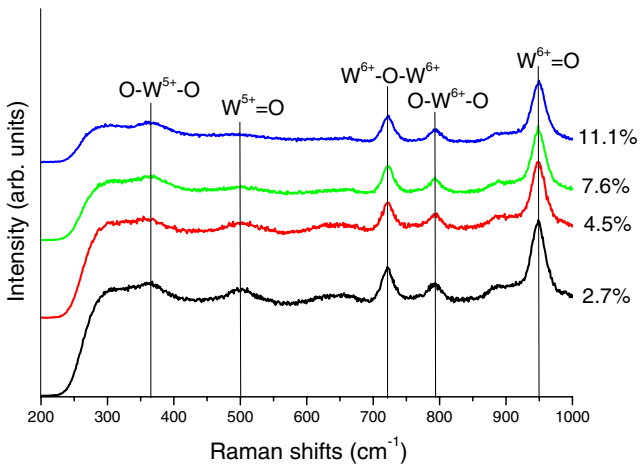

Fig. 4 Raman spectra of PET/ITO/WO_xC_y films synthesized by PECVD at various oxygen concentrations

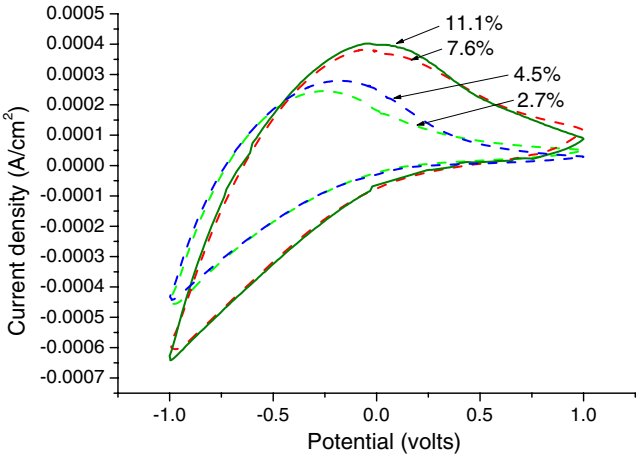

Fig. 5 Cyclic voltammograms of PET/ITO/WO_xC_y films synthesized by PECVD at various oxygen concentrations

The shape of the CV curve is governed by the appropriate equations relating to Li^+ ion diffusion. The diffusion coefficient of Li^+ ion during intercalation and de-intercalation can be calculated from the Randles–Sevick equation in Eq. 8 [24]:

$$i_p = 2.72 \times 10^5 n^{3/2} D^{1/2} C_0 v^{1/2} \quad (8)$$

where D denotes the diffusion coefficient (intercalation diffusion coefficient $D_{Li^+,i}$ and de-intercalation diffusion coefficient $D_{Li^+,d}$), C_0 denotes the concentration of active ions in the solution, v denotes the scan rate, n denotes the number of electrons and is assumed to be 1, and i_p denotes the peak current density (cathodic peak current density i_{pc}, anodic peak current density i_{pa}). Table 2 shows the highest $D_{Li^+,i}$ and $D_{Li^+,d}$ at 11.2×10^{-9} and 4.4×10^{-9} cm^2/s for Li^+ ion intercalation into and de-intercalation from the WO_xC_y films synthesized at optimal oxygen concentration of 7.6%, respectively. Highly declined values of $D_{Li^+,i}$ and $D_{Li^+,d}$ with decreases in oxygen concentrations to 2.7% and 4.5% were determined due to the greatly decreased values of i_{pc} and i_{pa}. Once the WO_xC_y films were synthesized at higher oxygen concentration of 11.1%, slight decreases in the values of $D_{Li^+,i}$ and $D_{Li^+,d}$ to 9.7×10^{-9} and 4.0×10^{-9} cm^2/s were obtained, respectively. This is due to slight decreases in i_{pc} and i_{pa}. In this study, the promising values of $D_{Li^+,i}$ at 11.2×10^{-9} cm^2/s and $D_{Li^+,d}$ at 4.4×10^{-9} cm^2/s were measured at oxygen concentration of 7.6%, which is higher than the reported $\sim10^{-10}$ cm^2/s for glass/ITO/PECVD-synthesized WO_3 films [20], $\sim10^{-11}$ cm^2/s for glass/ITO/electroplated WO_3 films [25], and $\sim10^{-10}$ cm^2/s for glass/ITO/e-beam deposited WO_3 films [26].

The intercalation coefficient α_i of tungsten oxide $Li_{\alpha_i}WO_{3-z}$ is typically $0\leq\alpha_i\leq0.3$ [27]. Figure 6 shows Li^+ intercalation coefficient α_i and Li^+ de-intercalation coefficient α_d of WO_xC_y films synthesized on PET/ITO at various oxygen concentrations. At optimal oxygen concentration of 7.6%, high values of α_i and α_d of 0.09964 and 0.09498, respectively, were obtained. High values of α_i and α_d in Fig. 6 were found for the porous surface of WO_xC_y film observed in Fig. 2c. The porous surface of WO_xC_y film allows Li^+ ions to easily intercalate into and de-intercalate from the WO_xC_y films. Lower values of α_i and α_d were observed in Fig. 6 as oxygen concentration was set to higher or lower than 7.6%, resulting in less porous surfaces as revealed in Fig. 2a, b, and d.

Electrochromic performance

The transmittance spectra of the PET/ITO/WO_xC_y just after WO_xC_y film deposition, and following Li^+ intercalation into WO_xC_y film (coloring state in blue) and Li^+ de-intercalation out from WO_xC_y film (bleaching state in transparent) are shown in Fig. 7a–d. Figure 7a shows that the film deposited at lower oxygen concentration of 2.7% offers much lower transmittance values of 42.7% and 33.7% at wavelengths of 550 and 650 nm, respectively. Once oxygen concentration increased to 4.5–11.1%, the transmittance values respectively increased to 50.3–90.5% and 43.8–96.8% at wavelengths of 550 and 650 nm, as shown in Fig. 7b. After Li^+ was intercalated from 0.1 M $LiClO_4$–PC electrolyte to the surfaces of WO_xC_y films, WO_xC_y films turned blue, which resulted in the much decreased transmittance of PET/ITO/WO_xC_y, as shown in Fig. 7a–d. Once Li^+ was de-

Table 2 Electrochemical properties of PET/ITO/WO_xC_y films associated with intercalation and de-intercalation of Li^+ ions at various oxygen concentrations

Oxygen concentration (%)	Li^+ intercalation				Li^+ de-intercalation			
	i_{pc} (mA/cm^2)	E_{pc} (V)	Q_i (mC/cm^2)	$D_{Li+,i}$ (10^{-9} cm^2/s)	i_{pa} (mA/cm^2)	E_{pc} (volt)	Q_d (mC/cm^2)	$D_{Li+,d}$ (10^{-9} cm^2/s)
2.7	0.44	−0.989	5.4	5.3	0.25	−0.260	4.9	1.6
4.5	0.45	−0.989	5.2	5.6	0.28	−0.176	5.3	2.1
7.6	0.64	−0.998	10.7	11.2	0.40	−0.044	10.2	4.4
11.1	0.60	−0.976	8.9	9.7	0.38	−0.050	8.7	4.0

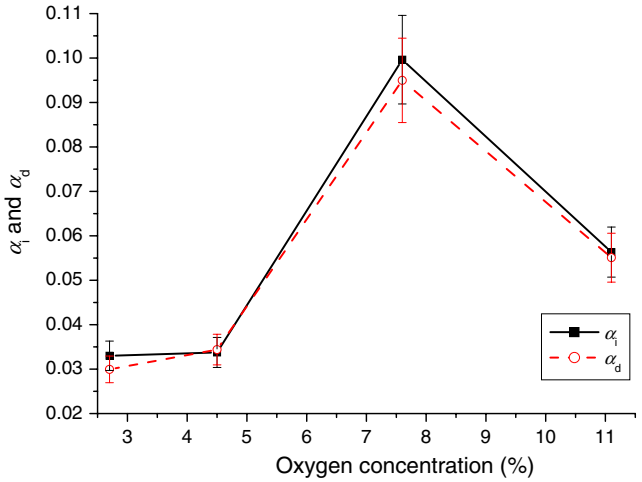

Fig. 6 Intercalation coefficient α_i and de-intercalation coefficient α_d of Li^+ ions into/out from PET/ITO/WO_xC_y films as a function of oxygen concentration

intercalated from the surfaces of $Li_{\alpha_i}WO_xC_y$ films to 0.1 M $LiClO_4$–PC electrolyte, WO_xC_y films were bleached to transparency, which resulted in the significantly decreased transmittance of PET/ITO/WO_xC_y, as shown in Fig. 7a–d. The transmittances of the PET/ITO/WO_xC_y increased after going from colored (light blue) to bleached (transparent) states. If an optimal oxygen concentration of 7.6% was applied for synthesis, Fig. 7c shows that the transmittance values of 29.5% and 21.8% for coloring increased dramatically to 95.2% and 94.7% at wavelengths of 550 and 650 nm, respectively, while bleaching.

The electrochromic performance of the PET/ITO/WO_xC_y was characterized by transmittance variation ΔT, optical density change ΔOD, and color efficiency η at wavelengths of 550 and 650 nm as a function of oxygen concentration. Figure 8 shows the low values for transmittance variation ΔT of 11.0–36.6% and 8.5–33.8% at wavelengths of 550

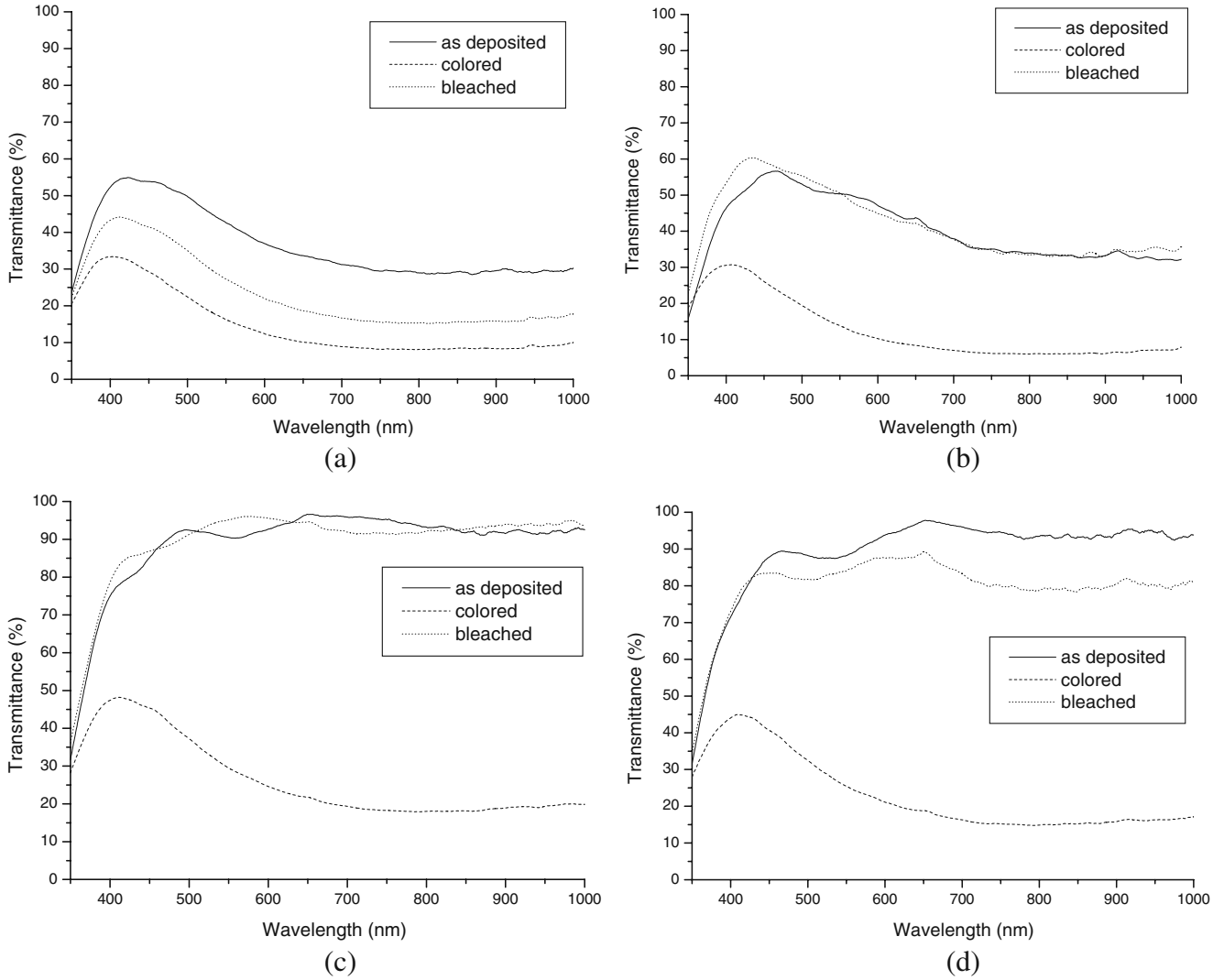

Fig. 7 The transmittance spectra of as-deposited, bleached, and colored PET/ITO/WO_xC_y films synthesized by PECVD at oxygen concentrations of **a** 2.7%, **b** 4.5%, **c** 7.6%, and **d** 11.1% plotted as a function of wavelength

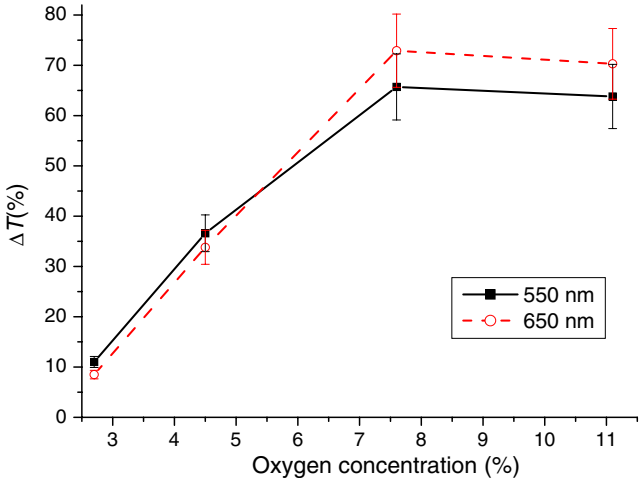

Fig. 8 The transmittance variation (ΔT) of PET/ITO/WO_xC_y films synthesized by PECVD as a function of oxygen concentration at wavelengths of 550 and 650 nm

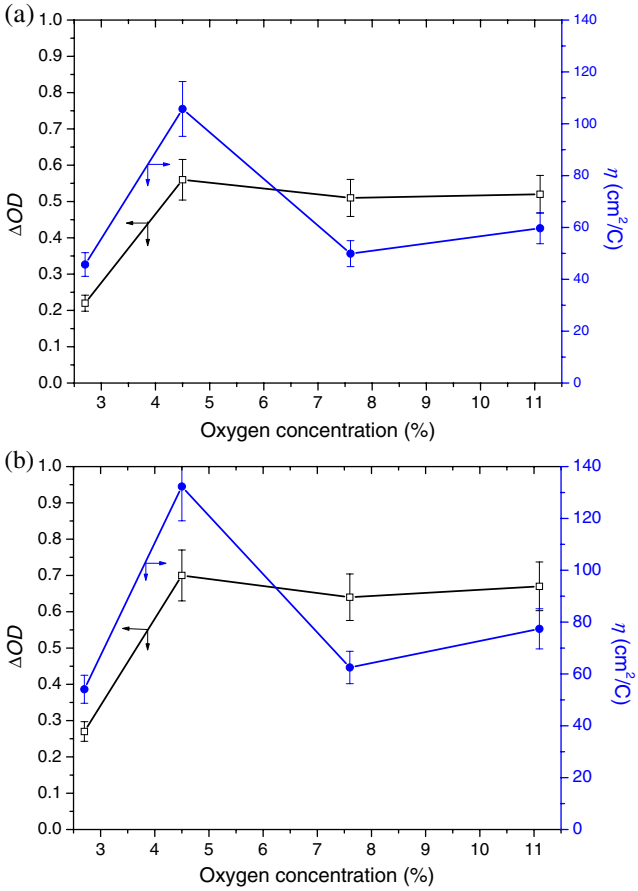

Fig. 9 The optical density change (ΔOD) and color efficiency (η) of PET/ITO/WO_xC_y films synthesized by PECVD as a function of oxygen concentration at wavelengths of **a** 550 nm and **b** 650 nm

and 650 nm, respectively, obtained using the lowest oxygen concentrations of 2.7–4.5%. With an optimal oxygen concentration of 7.6% for synthesis, the highest values of transmittance variation ΔT were 65.7% and 72.9% at wavelengths of 550 and 650 nm, respectively. Bessiere et al. [28] stated that the transmittance variation ΔT for WO_x films deposited onto flexible PET/ITO substrate by sol–gel deposition is up to 20% at a wavelength of 630 nm. In our previous studies [11, 29], the transmittance variation ΔT for WO_x films deposited onto flexible PET/ITO substrate by sputtering was up to 62–73.1% at a wavelength of 650 nm. Hence, this study offered an excellent transmittance variation ΔT of 72.9% at a wavelength of 650 nm for depositing WO_xC_y films onto flexible PET/ITO substrate by PECVD.

For electrochromic windows, the required contrast ratio is from 4:1 to 10:1 [30]. The contrast ratio is calculated as the ratio of the transmittance of an electrochromic device in a bleached state (ion de-intercalation state) T_{bleached} (%) to the transmittance of the sample in a colored state (ion intercalation state) T_{colored} (%). The optical density change ΔOD can be calculated from the logarithm of the contrast ratio. Optical density change ΔOD of 0.6 to 1 is required for an electrochromic window. Figure 9a–b shows that higher optical density change ΔOD was obtained at wavelengths of 550 and 650 nm as WO_xC_y films were synthesized onto flexible PET/ITO substrate by PECVD at higher oxygen concentrations of 4.5–11.1%. Figure 9b shows the acceptable optical density change ΔOD of 0.64–0.70 at a wavelength of 650 nm with higher oxygen concentrations of 4.5–11.1%.

One of the most important criteria for selecting electrochromic materials is the coloration efficiency η, which is defined as the change in optical density (ΔOD) divided by the intercalated charge per unit area (q). High coloration efficiency η can provide a large optical modulation with small charge intercalation (or de-intercalation) and is a crucial parameter for practical electrochromic devices. Figure 9a–b shows the highest coloration efficiencies η of 105.7 and 132.3 cm^2/C obtained at wavelengths of 550 and 650 nm, respectively, as WO_xC_y films were synthesized onto flexible PET/ITO substrate by PECVD at an oxygen concentration of 4.5%. The highest coloration efficiency η was obtained at an oxygen concentration of 4.5%, due to the highest change in optical density (ΔOD), as shown in Fig. 9a–b, and lower de-intercalated charge per unit area (q) of 5.3 mC/cm^2, as shown in Table 1. However, low values for transmittance variation ΔT of 36.6% and 33.8% at wavelengths of 550 and 650 nm, respectively, were measured, as shown in Fig. 8. Figure 9a–b shows that coloration efficiencies η of 49.9–59.7 and 62.5–77.5 cm^2/C were obtained at wavelengths of 550 and 650 nm, respectively, as WO_xC_y films were synthesized onto flexible PET/ITO substrate by PECVD at higher oxygen concentrations of 7.6–11.1%. Brigouleix et al. [15] reported that the coloration efficiency η of electrochromic WO_{3-z} films

Table 3 Atomic compositions of WO_xC_y films synthesized by PECVD at various oxygen concentrations

Oxygen concentration (%)	C (%)	O (%)	W (%)
2.7	42.08±4.21	44.61±4.46	13.31±1.33
4.5	33.49±3.35	49.36±4.94	17.15±1.72
7.6	31.44±3.14	51.17±5.12	17.39±1.74
11.1	29.44±3.00	52.98±5.30	17.58±1.76

deposited onto flexible PET/ITO substrate by pulsed dc magnetron sputtering is up to 40 cm^2/C. Hence, this study provided promising coloration efficiency η for deposition of WO_xC_y films onto flexible PET/ITO substrate by PECVD.

Surface compositions and oxygen deficiency

The atomic compositions of carbon (C), oxygen (O), and tungsten (W) in PECVD-synthesized WO_xC_y film were determined by the proportions of the corrected intensity area for the XPS spectra of C_{1s}, O_{1s}, and W_{4f}. The corrected intensity areas of C_{1s}, O_{1s}, and W_{4f} were obtained by dividing the intensity areas of XPS spectra for C_{1s}, O_{1s}, and W_{4f} by their relative sensitivity factors of 1, 2.93, and 9.8. The atomic compositions of nitrogen (N) for PECVD-synthesized WO_xC_y films were found to be less than 0.5%, which is beyond the resolution of XPS. Nitrogen (N) incorporating deposition of WO_xC_y films was negligible in this study. Table 3 shows the atomic compositions of PECVD-synthesized WO_xC_y films at various oxygen concentrations. The lower the oxygen concentration in plasmas, the higher the carbon composition, and the lower the oxygen composition in WO_xC_y films, which resulted in lower transmittance value of as-deposited WO_xC_y films, as shown in Fig. 7a–d.

Berggren et al. [31] reported that the color of substoichiometric films in the tungsten oxide WO_x range is dependent on their x values, i.e., very transparent if ~2.75≤x≤3.0 and blue if x≤~2.75. This study investigated how the x and y values affected the electrochromic performance of WO_xC_y films. The x and y values were calculated by taking the individually corrected intensity areas of C_{1s} and O_{1s} and dividing each by the corrected intensity area of W_{4f}, as shown in Table 4. Table 4 shows that the x values for WO_xC_y films at oxygen concentrations of 2.7%, 4.5%, 7.6%, and 11.1% were 3.35, 2.88, 2.97, and 3.01, respectively. Those x values were higher than 2.75. However, some black color (low transmittance values in Fig. 7a–b) was observed on as-deposited WO_xC_y films at oxygen concentrations of 2.7% and 4.5%. This is due to the high y values of 3.16 and 1.96 (see Table 4) observed at oxygen concentrations of 2.7% and 4.5%, respectively.

When Li^+ ions and electrons flow into the WO_xC_y film, some W^{6+} ions are reduced to W^{5+} (see Fig. 1a) and polarize their surrounding lattice to form small polarons. Optical absorption is caused by small polaron transitions between two adjacent non-equivalent sites of tungsten (W^{5+} and W^{6+}) [32]. The electrochromic properties of PET/ITO/WO_xC_y in this study were dependent on the optical absorption of the small polaron transitions between two adjacent non-equivalent sites of tungsten (W^{5+} and W^{6+}). The higher the W^{5+} formed on the WO_xC_y films, the more Li^+ ions and electrons flowed into the WO_xC_y film, and the more W^{6+} on the WO_xC_y films were reduced to W^{5+}, which then polarized their surrounding lattice to form small polarons.

To find out the proportions of W^{5+} and W^{6+} on the surface of PET/ITO/WO_xC_y at oxygen concentrations of 2.7%, 4.5%, 7.6%, and 11.1%, the spectra in Fig. 10a were fitted after subtraction of Shirley background using Lorentzian (70%)–Gaussian (30%) product functions with full width at half maxima of 1.2 eV. The binding energies of the main doublet $W^{5+}_{4f5/2}$ and $W^{5+}_{4f7/2}$ for the W^{5+} core-level spectra of $WO_{2.5}$ were 36.4 and 33.9 eV, respectively. Thus, the binding energies of the main doublet $W^{6+}_{4f5/2}$ and $W^{6+}_{4f7/2}$ for W^{6+} core-level spectra of WO_3 were 37.2 and 35.1 eV, respectively. The x_1 value of $WO_{x_1}C_yO_{x_2}$ films can be found by taking the arithmetic average of the proportions of

Table 4 x and y values of WO_xC_y; z value of WO_{3-z}; x_1 and x_2 values of $WO_{x_1}C_yO_{x_2}$

Oxygen concentration (%)	WO_xC_y		WO_{3-z}	$WO_{x_1}C_yO_{x_2}$		
	x	y	z	$x_1=3-z$	$x_2=x-x_1$ (C–O)	$y-x_2$ (C–C)
2.7	3.35±0.34	3.16±0.32	0.18±0.02	2.82±0.28	0.73±0.07	2.43±0.24
4.5	2.88±0.29	1.95±0.20	0.14±0.01	2.86±0.29	0.02±0.01	1.93±0.19
7.6	2.97±0.30	1.81±0.18	0.12±0.01	2.88±0.29	0.09±0.01	1.72±0.17
11.1	3.01±0.30	1.67±0.17	0.09±0.01	2.91±0.29	0.10±0.01	1.57±0.16

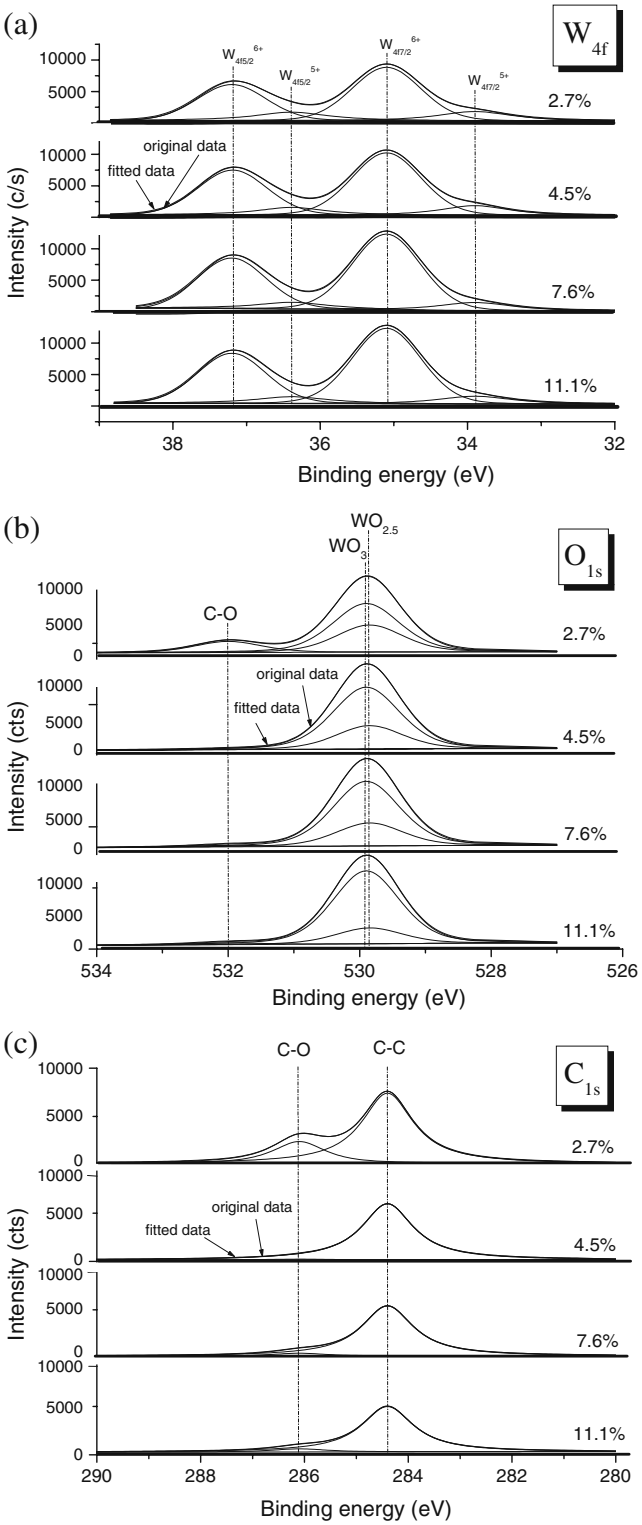

Fig. 10 **a** W_{4f}, **b** O_{1s}, and **c** C_{1s} spectra of PET/ITO/WO_xC_y films synthesized by PECVD at various oxygen concentrations plotted as a function of binding energy

WO_3 (W^{6+}) (which is 3) and $WO_{2.5}$ (W^{5+}) (which is 2.5), respectively. The x_2 value of $WO_{x_1}C_yO_{x_2}$ films can be calculated by $x_2=x-x_1$. x_1 and x_2 values of $WO_{x_1}C_yO_{x_2}$ films are shown in Table 4. x_1 value of $WO_{x_1}C_yO_{x_2}$ films can be referred to as $3-z$ of WO_{3-z} films. The z value is the so-called oxygen deficiency z of WO_{3-z} films. Higher values of oxygen deficiency z make more sites available for electron and Li^+ double insertions.

The x_2 value of $WO_{x_1}C_yO_{x_2}$ films can be referred to as the proportion of chemical bond C–O. Figure 10b–c verifies that chemical bond C–O is formed in $WO_{x_1}C_yO_{x_2}$ films. Then, the $y-x_2$ value for $WO_{x_1}C_yO_{x_2}$ films can be referred to as the proportion of chemical bond C–C, as shown in Table 3. Figure 10c proves that chemical bond C–C is created in $WO_{x_1}C_yO_{x_2}$ films. In this study, the chemical bonds such as C–C and C–O formed in $WO_{x_1}C_yO_{x_2}$ films were used to prevent cracking created in $WO_{x_1}C_yO_{x_2}$ films after 180° bending tests for 500 cycles. Lee et al. [22] reported that the oxygen deficiency z in a-WO_{3-z} (amorphous tungsten oxide) can vary between 0 and 0.5. They also concluded that the electrochromic performance increases with increasing oxygen deficiency (up to 0.3) in a-WO_{3-z} and no coloration is observed in nearly stoichiometric films (z=0.02). In this study, the microstructures of WO_xC_y films were found to be amorphous, as confirmed by the X-ray diffraction data, but the data are not presented here. The higher the proportion of W^{5+} on WO_xC_y films, the lower the x_1 value of $WO_{x_1}C_yO_{x_2}$ films, and the higher the oxygen deficiency z on $WO_{3-z}C_yO_{x_2}$ films. The proportions of W^{5+} and W^{6+} on the surfaces of PET/ITO/WO_xC_y at various oxygen concentrations are shown in Fig. 11. The lower the oxygen concentration, the higher the proportion of W^{5+}, and the lower the proportion of W^{6+}. Higher proportions of W^{5+} make more sites available for

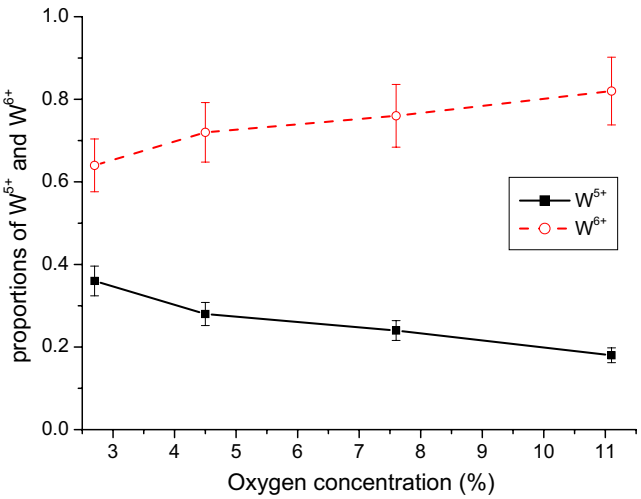

Fig. 11 The proportions of W^{5+} and W^{6+} on the surfaces of PECVD-synthesized WO_xC_y films as a function of oxygen concentration

Li^+ and electron double intercalations. Hence, the lower the oxygen concentration, the more sites that are available for electron and Li^+ double intercalations. However, WO_xC_y films deposited at low oxygen concentrations of 2.7% and 4.5% provide low values of intercalation coefficient α_i (see Fig. 6) since the chemical bonds C–C and C–O on WO_xC_y films hinder the Li^+ ion intercalation for high $y-x_2$ and x_2 values, as shown in Table 4. Once the oxygen concentration is set at 4.5–11.1%, the proportions of chemical bond C–O (x_2 value in Table 4) are negligible at 0.02–1.0. When the oxygen concentration is increased from 4.5% to 7.6%, the proportion of chemical bond C–C ($y-x_2$ value in Table 4) decreases from 1.93 to 1.72, while the proportion of W^{5+} decreases from 0.28 to 0.24. The values of intercalation coefficient α_i and de-intercalation coefficient α_d increased from 0.03375 and 0.00344 to 0.09964 and 0.09498 (see Fig. 6) after Li^+ ion intercalation and de-intercalation, respectively, due to less hindrance by chemical bond C–C. The porous surface of WO_xC_y film synthesized at oxygen concentration of 7.6%, shown in Fig. 2c, allows Li^+ ions to be easily intercalated into and de-intercalated from the films. When the oxygen concentration further increased to 11.1%, the proportion of chemical bond C–C ($y-x_2$ value in Table 4) decreased to 1.57, though the proportion of W^{5+} decreased to 18%. However, the values of intercalation coefficient α_i and de-intercalation coefficient α_d then decreased to 0.05634 and 0.05508 (see Fig. 6) after Li^+ ion intercalation and de-intercalation, even though there was less hindrance by chemical bond C–C. This is due to the less porous surface (see Fig. 2d) and lower oxygen deficiency z (see Table 4) of WO_xC_y ($WO_{3-z}C_yO_{x_2}$) film synthesized at oxygen concentration of 11.1%.

Conclusions

PECVD-synthesized WO_xC_y film with noteworthy light modulation of 72.9% transmittance variation and coloration efficiency of 62.5 cm^2/C was achieved at a wavelength of 650 nm after Li^+ intercalation and de-intercalation in 0.1 M $LiClO_4$–PC electrolyte. This was due to porous surface, high x value, low proportions of C–C and C–O chemical bonds, and high oxygen deficiency z. The porous surface allows Li^+ to be inserted into and extracted from WO_xC_y film easily. High x value and low proportions of chemical bonds C–C and C–O assure transparent WO_xC_y film. High oxygen deficiency z results in high amount of Li^+ intercalation into and de-intercalation out from WO_xC_y film.

Acknowledgements This study was supported by the National Science Council of the Republic of China (NSC96-2221-E-035-121 and NSC97-2221-E-035-046).

References

1. Deb SK (2008) Sol Energ Mater Sol Cell 92:245
2. Granqvist CG (2006) Nature Mater 5:89
3. Tajima K, Yamada Y, Bao YS, Okada M, Yoshimura K (2008) J Appl Phys 103:013512
4. Rauh RD (1999) Electrochim Acta 44:3165
5. Granqvist CG, Avendano E, Azens A (2003) Thin Solid Films 442:201
6. Faughnan BW, Crandall RS, Heyman PM (1975) RCA Review 36:177
7. Djaoued Y, Priya S, Balaji S (2008) J Non-Cryst Solids 354:673
8. Srivastava AK, Deepa M, Singh S, Kishore R, Agnihotry SA (2005) Solid State Ionics 176:1161
9. Sivakumar R, Raj AME, Subramanian B, Jayachandran M, Trivedi DC, Sanjeeviraja C (2004) Mater Res Bull 39:1479
10. Sivakumar R, Gopalakrishnan R, Jayachandran M, Sanjeeviraja C (2007) Opt Mater 29:679
11. Lin YS, Chiang YL, Lai JY (2009) Solid State Ionics 180:99
12. Baserga A, Russo V, Di Fonzo F, Bailini A, Cattaneo D, Casari CS, Li Bassi A, Bottani CE (2007) Thin Solid Films 515:6465
13. Dillon AC, Mahan AH, Deshpande R, Parilla PA, Jones KM, Lee SH (2008) Thin Solid Films 516:794
14. Tracy CE, Benson DK (1986) J Vac Sci Technol A 4:2377
15. Brigouleix C, Topart P, Bruneton E, Sabary F, Nouhautm G, Campet G (2001) Electrochim Acta 46:1931
16. Leftheriotis G, Papaefthimiou S, Yianoulis P (2004) Sol Energ Mater Sol Cell 83:115
17. Lin YS, Chen CL (2008) Plasma Process Polym 5:471
18. Lee SH, Cheong HM, Liu P, Smith D, Tracy CE, Mascarenhas A, Pitts JR, Deb SK (2001) Electrochim Acta 46:1995
19. Filipescu M, Ossi PM, Santo N, Dinescu M (2009) Appl Surf Sci 255:9699
20. de Wijs GA, de Groot RA (2001) Electrochim Acta 46:1989
21. Orel B, Krasovec UO, Groselj N, Kosec M, Drazic G, Reisfeld R (1999) J Sol–Gel Sci Technol 14:291
22. Lee SH, Cheong HM, Tracy CE, Mascarenhas A, Czanderna AW, Deb SK (1999) Appl Phys Lett 75:1541
23. Fang G, Liu Z, Yao KL (2001) J Phys D 34:2260
24. Deepa M, Srivastava AK, Saxena TK, Agnihotry SA (2005) Appl Surf Sci 252:1568
25. Vijayalakshmi R, Jayachandran M, Sanjeeviraja C (2003) Curr Appl Phys 3:171
26. Leftheriotis G, Papaefthimiou S, Yianoulis P (2007) Solid State Ionics 178:259
27. Niklasson GA, Granqvist CG (2007) J Mater Chem 17:127
28. Badilescu S, Ashrit PV (2003) Solid State Ionics 158:187
29. Lin YS, Chiang YL (2007) Plasma Process Polym 4:S89
30. Mathew JGH, Sapers SP, Cumbo MJ, O'Brien NA, Sargent RB, Raksha VP, Lahaderne RB, Hichwa BP (1997) J Non-Cryst Solids 218:342
31. Berggen L, Jonsson JC, Niklasson GA (2007) J Appl Phys 102:083538
32. Schirmer OF, Salje E (1980) Solid State Commun 33:333